Ultrafast ranging lidar based on real-time Fourier transformation

Haiyun Xia* and Chunxi Zhang

School of Instrument Science and Opto-Electronics Engineering, Beihang University, Beijing 100083, China
**Corresponding author: haiyunxia@126.com*

Received May 14, 2009; accepted May 26, 2009;
posted June 10, 2009 (Doc. ID 111100); published July 7, 2009

Real-time Fourier-transformation-based ranging lidar using a mode-locked femtosecond fiber laser is demonstrated. The object signal and the reference signal are guided from a fiber Mach–Zehnder interferometer into a dispersive element. The two optical pulses extend and overlap with each other temporally, which yields a microwave pulse on the photodetector with its frequency proportional to the time delay between the two signals. The temporal interferograms are transformed from the time domain into the frequency domain using a time-to-frequency conversion function obtained in the calibration process. The Fourier transform is used in the data processing. A range resolution of 334 nm at a sampling rate of 48.6 MHz over a distance of 16 cm is demonstrated in the laboratory. © 2009 Optical Society of America

OCIS codes: 120.0280, 120.3180, 140.4050, 140.3510, 280.3400, 320.7160.

Since the laser was invented, intensive research has been focused on its implementation in ranging and Doppler lidars based on either coherent or incoherent techniques [1,2]. Recently, optical ranging based on femtosecond laser became attractive for its inherent advantages, at least, as illustrated in the following four points. First, a mode-locked femtosecond laser could provide a large number of stable longitudinal modes with a narrow linewidth and uniform mode spacing [3]. The narrow linewidth of each longitudinal mode provides high resolution, while the selectable intermode beat-frequency ensures absolute ranging without ambiguity. Minoshima and Matsumoto reported a resolution of 50 μm by measuring the phase shift of a series of intermode beats based on a phasemeter [4]. Second, the repetition frequency of the mode-locked femtosecond lasers could be synchronized to an accurate microwave or rf clock directly. Also, the carrier-envelope phase slippage between successive pulses could be eliminated by using a self-referencing control technique [5,6]. Such characteristics extend the measurement to a coherent time of several seconds. Ye proposed to combine the time-of-flight technique and the fringe-resolved interferometry to achieve an absolute ranging over a long distance [7]. Third, a femtosecond laser generally has a spectral width broader than several nanometers. It is a good substitute for the traditional light source in a spectrally resolved white-light interferometry. Thus, Joo and Kim demonstrated a range resolution of 7 nm over a distance of 0.89 m [8]. Fourth, the working wavelength around 1.5 μm is compatible with the broad gain spectrum of the erbium-doped fiber amplifier (EDFA), which could be used to improve the signal-to-noise ratio in the optical receiver. Swann and Newbury reported a Doppler resolution of 0.12 m/s and a range resolution of 60 μm [9].

A temporal interferometric ranging lidar is proposed and demonstrated in this Letter. The schematic of the system is shown in Fig. 1. The optical source is a passively mode-locked femtosecond fiber laser (IMRA Femtolite 780 Model B-4-FC-PD), which emits a train of pulses with a pulse width of 394 fs (FWHM) and a center frequency of 192.31 THz at a repetition rate of 48.6 MHz. In the sensor module, the distance to be measured is incorporated into one arm of a fiber Mach–Zehnder interferometer (MZI) by using an optical fiber circulator and a fiber collimator. On the other arm of the MZI, an optical time delayer is used to change the time delay difference between the reference and the object signals. To perform a temporal interference, an in-line polarizer is added at the output end of the MZI. To achieve a largest fringe visibility in the interferogram, polarization controllers PC_1 and PC_2 are used to modulate the transmission of the two signals through the polarizer. A cooperative target (a reflecting mirror) is mounted on a nanopositioning stage (PI Model P-752.1CD) driven by a piezoelectric tube controller (PI Model E-665.CR). The nanopositioning system works in a servocontrol mode, which produces an accuracy of 0.2 nm. In the optical receiver two coils of dispersion-compensating fibers (DCFs)—DCF_1 and DCF_2—are used in cascade to stretch the femtosecond pulses sufficiently in the time domain. The optical pulses are amplified by

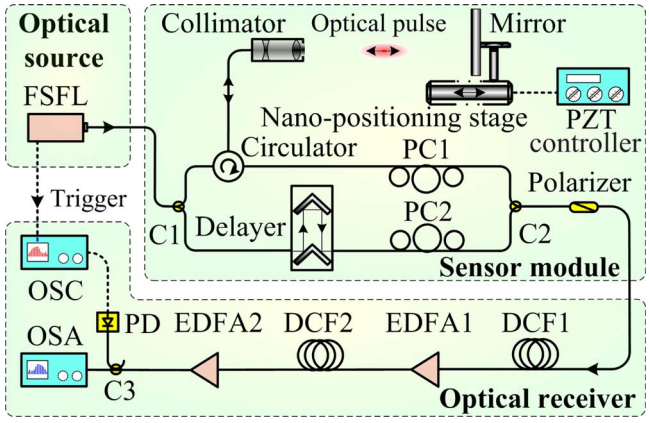

Fig. 1. (Color online) System layout. FSFL, femtosecond fiber laser; C, optical coupler; PC, polarization controller; PZT, piezoelectric tube; PD, photodetector.

$EDFA_1$ and $EDFA_2$ to guarantee the signal-to-noise ratio. The temporal interferogram and spectral interferogram are recorded using an oscillator (OSC) and an optical spectrum analyzer (OSA), respectively.

The chromatic dispersion in single-mode fibers has been proposed to implement a real-time dispersive Fourier transform [10]. If the femtosecond pulses and the DCF meet the condition $|T_0^2/\beta_2 L| \ll 1$, where T_0 is the pulse width of the femtosecond pulse, β_2 and L are the group-velocity dispersion (GVD) parameter and the total length of the DCF, and with the neglect of the higher-order dispersion, the temporal pulse passing through the DCF is a temporal analog of the spatial Fraunhofer diffraction [11],

$$\hat{a}_1(t) \propto \exp[jt^2/2\beta_2 L]\hat{A}_0(t/\beta_2 L), \tag{1}$$

where $\hat{A}_0(\omega)=|A_0(\omega)|\exp[i\varphi_0(\omega)]$ is the complex spectrum of the femtosecond pulse guided into the DCF. $I_0(\omega)=|A_0(\omega)|^2$ and $\varphi_0(\omega)$ are the spectral intensity and the phase of the pulse, respectively. So, the output information-bearing signal is proportional to the Fourier transform of the input information-bearing signal, with an angular frequency given by $\omega=t/\beta_2 L$.

For simplicity, the signals from the two arms of the MZI are supposed to be intensity equalized after passing through the polarizer. Thus, the impulse response of the sensor module is

$$h(t) = [\delta(t) + \delta(t+\tau)]/2, \tag{2}$$

where τ is the time-delay difference between the two arms of the MZI. The electrical field of the signal arriving at the photodetector can be expressed as a convolution $\hat{a}_2(t)=\hat{a}_1(t)*h(t)$. So, the output electric current is

$$i(t) = \Re\hat{a}_2(t)\cdot\hat{a}_2^*(t) = \tfrac{1}{4}\Re\{|A_0(\omega)|^2 + |A_0(\omega+\Delta\omega)|^2 + 2|A_0(\omega)||A_0(\omega+\Delta\omega)|\cos[\omega\tau+\Delta\varphi(\omega)]\}_{\omega=t/\beta_2 L}, \tag{3}$$

where $\Re$ is the responsivity of the photodetector, $\hat{a}_2^*(t)$ is the conjugate of $\hat{a}_2(t)$, $\Delta\omega=\tau/\beta_2 L$, and $\Delta\varphi(\omega)=\varphi(\omega)-\varphi(\omega+\Delta\omega)$. The pulses generated directly from the passively mode-locked femtosecond fiber laser are nearly transform limited, i.e., $\Delta\varphi(\omega)\approx 0$. And if $\Delta\omega$ is small enough, Eq. (3) can be approximated by

$$i(t) = \Re I_0(t/\beta_2 L)[1+\cos(\pi t/\beta_2 L)]/2. \tag{4}$$

In the frequency domain, the transfer function of the sensor module is $[1+\cos(\omega\tau)]/2$. The spectral interferogram recorded on the OSA is the product of the pulse spectrum and the transfer function

$$I(\omega) = \Re I_0(\omega)[1+\cos(\omega\tau)]/2. \tag{5}$$

From Eqs. (4) and (5), one can see that, by recording either the temporal interferogram or the spectral interferogram, τ can be retrieved.

Thanks to the high repetition rate of the femtosecond fiber laser, we perform a single-shot range detection based on the temporal interferogram. Under the effect of the third-order dispersion of the entire system and the unbalanced dispersion between the two arms of the MZI, the frequency of the temporal interferogram would change linearly with time. A detailed demonstration of this phenomenon is beyond the scope of this Letter. To calibrate the system, we scan the optical delayer in the reference arm until a temporal interferogram at a frequency of about 1 GHz is observed. The temporal interferogram and the spectral interferogram are recorded and shown along the abscissa and the ordinate, respectively, in Fig. 2. The peak centers of the two interferometric patterns are found using a single-peak fitting algorithm. To compensate the effect of the third-order dispersion and unbalanced dispersion in the MZI, a polynomial fitting function up to the second order, which relates the peak centers of the two patterns, is obtained,

$$f = 192.423 + 0.1293t + 1.958\times 10^{-4}t^2, \tag{6}$$

where the units of frequency and time are terahertz and nanoseconds, respectively.

We performed a relative displacement measurement in the following experiment. The distance from the collimator to the reflecting mirror is about 16 cm. The dynamic range is determined by the bandwidth of the oscilloscope (Tektronix Model TDS7704B, 7 GHz bandwidth), since the photodetector has a higher bandwidth (New Focus Model 1014, 45 GHz bandwidth). The temporal interferogram has a period of about $T_i=2\pi\beta_2 L/\tau$. Given the dispersion $DL=-960$ ps/nm, the center wavelength $\lambda=1559$ nm, and with the relation $D=-2\pi c\beta_2/\lambda^2$, to satisfy the inequation $1/T_i<f_b$ ($f_b=7$ GHz) one can obtain $\tau<54.4$ ps. So the dynamic range is 8.17 mm. It is clear that, given a limited bandwidth of the receiver, the higher the dispersion DL, the larger the dynamic range. However, the stretched pulses should not overlap.

To initialize the system, we scan the optical delayer until a temporal interferogram with a frequency of about 3.5 GHz is detected. For a relative distance measurement, this position is set as the zero point. The frequency of the temporal interferogram is proportional to the time-delay difference linearly, so

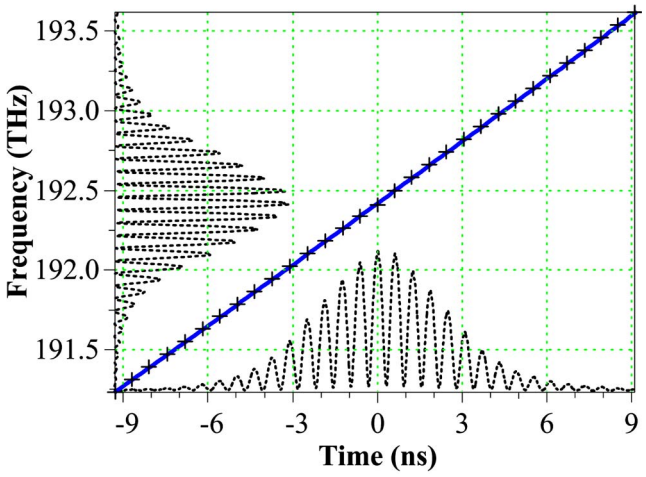

Fig. 2. (Color online) Time-to-frequency conversion function.

there is no ambiguity problem. We set the nanopositioning stage to nine different positions and record the temporal interferogram ten times at each position without averaging. The temporal interferograms recorded at the first position are shown in Fig. 3(a). After the data acquisition, each temporal interferogram is aligned to the center of the carrier envelope and transformed from the time domain to the frequency domain using Eq. (6), then rescaled by using spline interpolation and resampling, followed by an inverse Fourier transformation. The final results are shown in Fig. 3(b). The main sideband is associated with the time-delay difference. Some minor sidebands are also observed, which may be associated with the backscattering of fiber connectors and the cross talk of the optical circulator used in the system. Since the envelope of the femtosecond pulse has a Gaussian shape, we fit each of the main sidebands to a Gaussian function with the center of each fitting result equal to the time delay difference. Finally, the relative displacement of the mirror can be calculated. The result is shown in Fig. 4. A standard deviation of 334 nm and a mean error of 85 nm are estimated from the 90 measurements.

Here, we demonstrated that the real-time Fourier transformation in an element that provides high GVD can be used to achieve an ultrafast range measurement. This method inherits the advantages from the accuracy of fringe encoding in both temporal and spectral interferometry techniques and from the resistance to noise in the Fourier processing. Attractively, the range information is encoded into the frequency of the generated microwave pulses. Thus, microwave techniques could be used to analyze the received signal instead of recording and processing the signal directly. Additionally, the all-fiber system shows high potential for integration. Although the dynamic range of this technique is small, we believe that it can be incorporated with other ranging techniques described at the beginning of this Letter to achieve a long distance measurement.

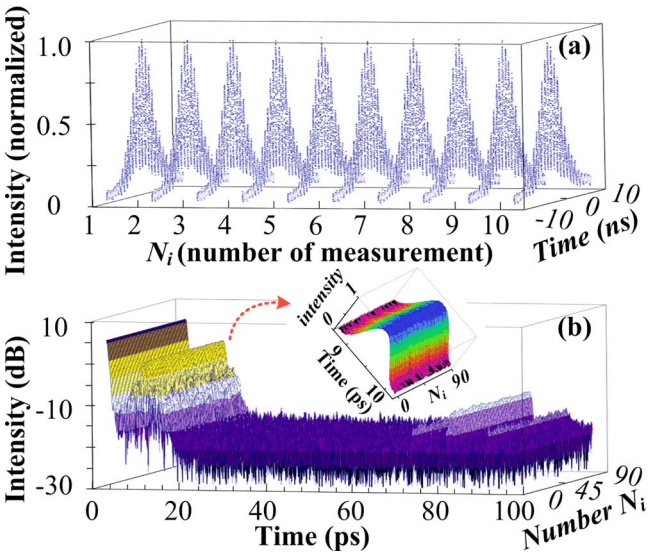

Fig. 3. (Color online) (a) Temporal interferograms recorded at the zero point, (b) inverse Fourier transform results shown on a logarithmic scale. Inset, partial view of the main sideband shown on a linear scale.

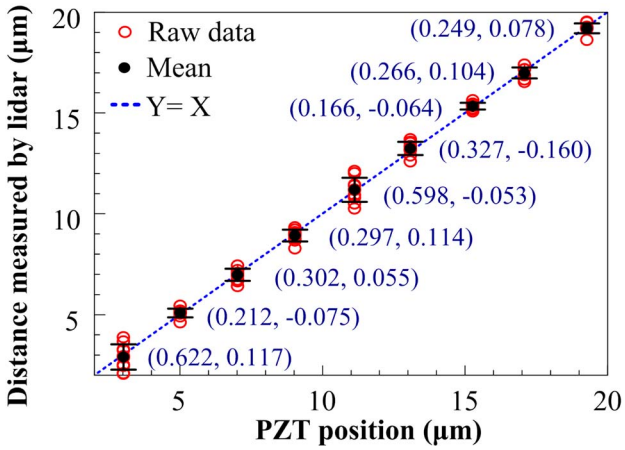

Fig. 4. (Color online) Comparison between the preset positions and the measurements. Data are shown in the format of (standard deviation, mean error).

The authors are grateful to Jianping Yao for his support in the experiments, and to the reviewers for their constructive comments. H. Xia is supported by the China Scholarship Council.

References

1. R. M. Huffaker and R. M. Hardesty, Proc. IEEE **84**, 181 (1996).
2. H. Xia, D. Sun, Y. Yang, F. Shen, J. Dong, and T. Kobayashi, Appl. Opt. **46**, 7120 (2007).
3. W. C. Swann, J. J. McFerran, I. Coddington, N. R. Newbury, I. Hartl, M. E. Fermann, P. S. Westbrook, J. W. Nicholson, K. S. Feder, C. Langrock, and M. M. Fejer, Opt. Lett. **31**, 3046 (2006).
4. K. Minoshima and H. Matsumoto, Appl. Opt. **39**, 5512 (2000).
5. D. J. Jones, S. A. Diddams, J. K. Ranka, A. Stentz, R. S. Windeler, J. L. Hall, and S. T. Cundiff, Science **288**, 635 (2000).
6. J. J. McFerran, W. C. Swann, B. R. Washburn, and N. R. Newbury, Opt. Lett. **31**, 1997 (2006).
7. J. Ye, Opt. Lett. **29**, 1153 (2004).
8. K.-N. Joo and S.-W. Kim, Opt. Express **14**, 5954 (2006).
9. W. C. Swann and N. R. Newbury, Opt. Lett. **31**, 826 (2006).
10. T. Jannson, Opt. Lett. **8**, 232 (1983).
11. A. Papoulis, J. Opt. Soc. Am. A **11**, 3 (1994).